Dynamic drag modeling of submerged aquatic vegetation canopy flows

T.I. Marjoribanks & R.J. Hardy
Durham University, Durham, UK

S.N. Lane
UNIL Lausanne, Switzerland

D.R. Parsons
University of Hull, Hull, UK

ABSTRACT: Vegetation has a profound effect on flow and sediment transport processes in natural rivers, by increasing both skin friction and form drag. The increase in drag introduces a drag discontinuity between the in-canopy flow and the flow above, which leads to the development of an inflection point in the velocity profile, resembling a free shear layer. Therefore, drag acts as the primary driver for the entire canopy system. Most current numerical hydraulic models which incorporate vegetation rely either on simple, static plant forms, or canopy-scaled drag terms. However, it is suggested that these are insufficient as vegetation canopies represent complex, dynamic, porous blockages within the flow, which are subject to spatially and temporally dynamic drag forces. Here we present a dynamic drag methodology within a CFD framework. Preliminary results for a benchmark cylinder case highlight the accuracy of the method, and suggest its applicability to more complex cases.

1 INTRODUCTION

Aquatic, in-channel vegetation acts as a control on river corridor form and dynamics (Gurnell, 2013), affecting conveyance (Nepf et al., 2007, Jarvela, 2002), sediment dynamics (Sand-Jensen et al., 1989, Sukhodolov and Sukhodolova, 2010) and habitat development (Lopez and Garcia, 2001, Liu and Shen, 2008). Effective river management requires a good understanding of these effects, and the ability to predict, with accuracy, the local impact of vegetation on flow and river channel morphology (Stoesser et al., 2009).

Current reach-scale (e.g. Fischer-Antze et al., 2001, Lopez and Garcia, 2001, Defina and Bixio, 2005) as well as higher resolution (e.g. Abdelrhman, 2007, Dijkstra and Uittenbogaard, 2010) numerical models for vegetated flows rely upon empirical drag coefficients. The prime purpose of such coefficients is to add a bulk resistance to the flow, rather than account for complexity related to plant form or local flow variations. This is a significant limitation, particularly for complex vegetation canopies

Here we present a new methodology for directly calculating drag forces within high resolution vegetation models. This method removes the need for empirical drag coefficients, increasing accuracy and allowing the spatial and temporal effects of drag to be characterized.

2 DRAG WITHIN VEGETATED CHANNELS

Individual vegetation elements within the flow represent significant additional sources of viscous skin friction drag (Nikora and Nikora, 2007), resulting from the increased boundary surface areas and form drag as a result of flow diversion and separation (Raupach and Thom, 1981). Thus, vegetation stems extract energy from the mean flow, via drag, converting it into both stem wake-scale turbulence as well as directly into heat (Zong and Nepf, 2010, Yagci and Kabdasli, 2008). The fraction of energy which is converted into turbulent kinetic energy depends on the ratio of form and viscous drag, which in turn is dependent on the plant morphology, plant biomechanics and flow conditions (Nepf, 1999). For typical aquatic macrophytes, stem diameter is small (<0.01 m) and therefore any stem-scale turbulence quickly dissipates into heat (Seginer et al., 1976).

The result of this increased drag within the canopy is a drag discontinuity between the canopy flow and the flow above (Nepf et al., 2007). This leads to a reduced velocity within the canopy and the development of an inflection point in the velocity profile between the two flow regions (Raupach et al., 1996, Ikeda and Kanazawa, 1996). This inflected velocity profile is unstable and leads to the generation of canopy-scaled turbulent structures (Ghisalberti and Nepf, 2002, Nezu and Onitsuka, 2001, Finnigan, 2000) which develop into roller vortices which dom-

inate the turbulent kinetic energy budget (Nepf and Ghisalberti, 2008). The frequency of these vortices relates directly to the shape of the inflected velocity profile (Ho and Huerre, 1984) which depends in turn upon the scale of the drag discontinuity (Nepf et al., 2007, Nepf and Ghisalberti, 2008).

These turbulent structures may then interact with the vegetation canopy in two ways. First, large-scale turbulent structures can cause plant motion, which in turn can affect canopy turbulence, through either modulating (Finnigan, 1979) or dampening (Wilson et al., 2003) vortices. Second, canopy vegetation can exert drag on the turbulent flow as well as the mean flow. This transfers energy from the large-scale to the small (wake) scale, bypassing the intermediate scales. This creates a spectral shortcut phenomenon (Finnigan, 2000), altering the energy cascade within the channel.

Thus, stem-scale drag acts as the driver of canopy flows, dictating the velocity profile, turbulence characteristics and plant motion. It is important therefore, that models designed to replicate vegetated channels represent vegetative drag adequately at the stem-scale.

3 CURRENT METHODS FOR DRAG MODELLING

Typically, drag is calculated using the standard drag equation (Equation 1).

$$F_D = \frac{1}{2}\rho C_D A_f u^2 \quad (1)$$

This equation relates the drag force to the fluid density (ρ), the plant frontal area (A_f), the local fluid velocity (u) and the drag coefficient (C_D). Thus, it represents a function of both local flow and vegetation conditions.

Application of this equation requires quantification of C_D, the drag coefficient. Classical fluid dynamics experiments have led to a good understanding of C_D values for simple shapes such as cubes, plates and cylinders. However, even for such simple shapes C_D exhibits a flow dependence. For example, the variation in C_D with Reynolds number for cylinders has been well documented (Tritton, 1988, Roshko, 1961, Tritton, 1959) and this relationship is shown within the experimental data in Figure 1.

Many current vegetation models utilize this relationship by approximating vegetation stalks as rigid cylinders (Fischer-Antze et al., 2001, López and García, 1998, Stoesser *et al*., 2006). For the Reynolds numbers experienced in most open-channel flows (10^3 to 10^6), this results in a C_D value of 1 (Figure 1). This approach is attractive from a modelling perspective as it provides a simple approach for estimating vegetative drag and has therefore been used across a range of models which can be broadly summarized within two categories.

Firstly, a number of canopy-scale vegetation models have been developed, which treat each vegetation stem as a sub-grid blockage and calculate the net drag force exerted on the flow, based upon a characteristic cylinder diameter, and stem density (Defina and Bixio, 2005, Fischer-Antze et al., 2001, Lopez and Garcia, 2001). Accordingly, bulk sink and source terms are added into the Navier-Stokes momentum equations to account for the effect of the vegetation on the mean and turbulent flow. These models enable simulation of canopies with large extent without the need for high resolution, computationally expensive modelling strategies. However, as they rely upon pre-defined drag coefficients, they are only applicable for heterogeneous canopies with simple, cylindrical plant form. Furthermore, while they have been shown to reproduce mean flow quantities well, they perform less well at predicting turbulence (Defina and Bixio, 2005).

Secondly, stem-scale vegetation models have been developed which resolve each vegetation stem explicitly. Within this class of model, there are two separate types: those which fully solve the flow field using computational fluid dynamics (CFD), and those which use a simplified flow model. Within the existing body of research, full CFD models have been restricted mainly to rigid vegetation. Stoesser *et al.* (2006) performed numerical experiments on flow through an array of cylinders, replicating previous experimental results well. Such high resolution experiments have the benefit that the form drag is explicitly resolved and there is therefore no need to use drag coefficients. However, within this model there is no flow-vegetation interaction and therefore the vegetation is considered as a rigid, rather than flexible, object. The model is therefore unable to capture flow-vegetation feedbacks with can influence canopy processes (Nepf and Ghisalberti, 2008, Okamoto and Nezu, 2009).

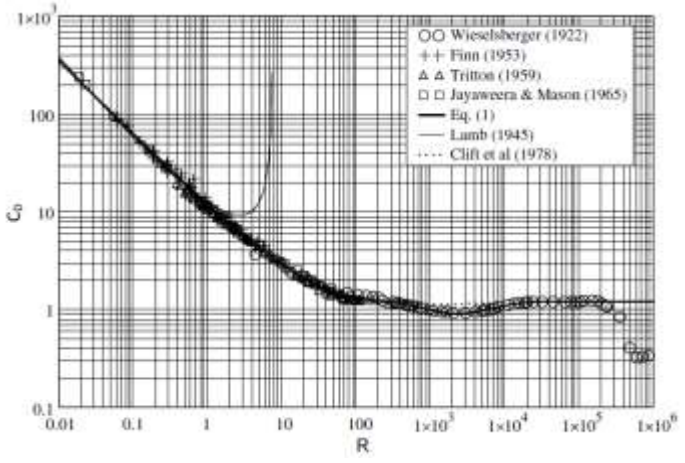

Figure 1: Experimental data showing the change in drag coefficient with Reynolds number for flow around a cylinder Figure reproduced from Cheng (2013) with permission from ASCE.

Plant reconfiguration into a more streamlined form is a key drag-reduction strategy (Sand-Jensen, 2003) employed by natural macrophytes and is therefore important to include within vegetation models. This reconfiguration can occur from the leaf scale right through to the patch scale (Albayrak et al., 2011) and will affect the plant frontal area, as well as the drag coefficient. Thus, for aquatic vegetation it is important to quantify the drag coefficient for more streamlined shapes than rigid cylinders.

Abdelrhman (2007) developed a model which accounted for flexible vegetation, and thus change in frontal area, but his model used a single predetermined drag coefficient. Furthermore, the model was implemented within a simplified flow model.

Dijkstra and Uittenbogaard (2010) developed a more complex model which used a plant angle-dependent drag coefficient, values of which had been obtained experimentally. This variable drag coefficient represents a significant improvement compared to a constant drag coefficient value, however still fails to fully account for spatial variability in drag throughout the canopy. Effects such as sheltering within the canopy can lead to large spatial variations in drag throughout the canopy (Raupach and Thom, 1981).

Reviewing current methods, it is clear that at present, the majority of stem-scale and canopy-scale flow-vegetation models rely upon the assumption of rigid, cylindrical vegetation, or upon pre-defined, empirical drag coefficient values, which are not transferable between plant types or flow conditions. Therefore, there is the need for a drag calculation method which does not rely upon *a priori* knowledge of the drag coefficient and which allows accurate calculation of canopy-induced drag forces across a range of conditions. Such a method is outlined below.

4 METHODOLOGY

In this study, high resolution numerical modelling was undertaken in order to resolve the flow dynamics explicitly and derive the drag coefficient from the results. There are therefore two key aspects to the methodology: the drag calculation method and the necessary CFD simulation.

4.1 *Drag Calculation Method*

The drag calculation method applied here assumes that the majority of the fluid drag will be form drag. This is a valid assumption for bluff objects, such as cylinders where 90-95% of the total drag is form drag and only a small component derives from skin friction drag (Lilly, 1967). However, it is noted that in cases where vegetation undergoes significant reconfiguration, this assumption may not be the case (Nikora and Nikora, 2007), and a separate additional skin friction drag treatment may have to be applied.

The drag calculation method applied here is based upon a pressure coefficient approach, which is a standard method, used within aerodynamics to calculate drag (Anderson, 1984). The drag is calculated by integrating the pressure acting upon the object over its entire surface area (A) to calculate the net force acting on the object. In doing so, the pressure must be resolved into the downstream direction in order to calculate the drag force acting in that direction (Figure 2).

If θ is the angle between the downstream direction and the surface normal at any given point on the surface area, then the drag force can be written in terms of the pressure (p) as

$$F_D = \int_A p \cos\theta \; dA. \tag{2}$$

Assuming a cylindrical vegetation form, this surface integral can be split into two separate integrals (Equation 3), one over the angle θ and the other over the cylinder height (h).

$$F_D = \int_0^h \int_0^{2\pi} p \cos\theta \; r_p d\theta dh. \tag{3}$$

Here, r_p is the vegetation radius. Applying this to the case of a numerical model, dh becomes the cell height, over which the pressure is assumed to be constant. Similarly, the circumference of the stalk is discretised into a number of boundary cells, each of which contains an approximation of the pressure at the fluid-vegetation boundary.

Thus, equation 3 can be discretised using the trapezium rule into a form which refers to specific resolved pressure values, $P_i=(p-p_\infty)cos\theta$.

$$F_D = rh \sum_{i=1}^{n} \frac{1}{2}(P_{i+1} + P_i)(\theta_{i+1} - \theta_i) \tag{4}$$

Here p_∞ is the free-stream pressure, and P_i and θ_i values are evaluated within each of the n boundary cells.

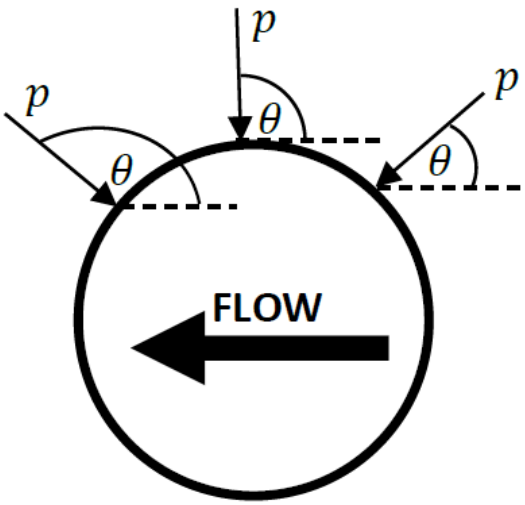

Figure 2; Schematic of resolved pressure around the cylindrical stem. Here, individual surface pressure values (p), are resolved into the downstream direction.

Equation 4 can then re-arranged to solve for the drag coefficient by substituting in the pressure coefficient:

$$C_P = \frac{p-p_\infty}{0.5\rho U^2} \quad (5)$$

This gives:

$$C_D = \sum_{i=1}^{n} \frac{1}{2\pi}\left(C_{P,i+1}\cos\theta_{i+1} + C_{P,i}\cos\theta_i\right)\Delta\theta \quad (6)$$

Here, $\Delta\theta$ is the local difference in θ between neighboring nodes. This formulation only applies to the case of cylindrical plant forms but could be extended to incorporate a wider range of plant forms by considering the sum of the forces over each face, resolved according to its relative orientation. Using this method, providing high resolution pressure data is available, it is possible to back-calculate the drag force and coefficient.

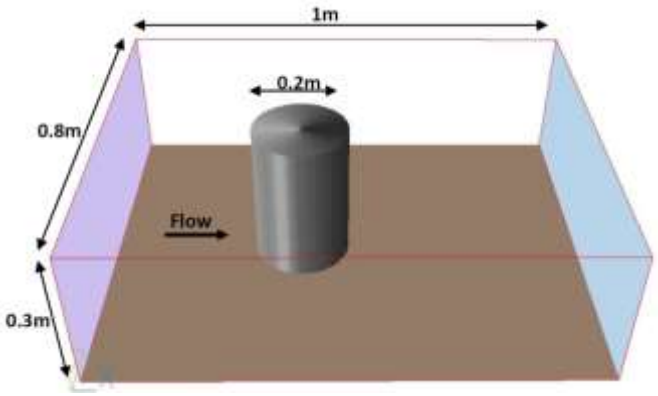

Figure 3: Numerical simulation setup for the benchmark test.

4.2 *Simulation setup*

In order to validate the drag calculation methodology described above, a high resolution numerical experiment was undertaken, of flow around a cylinder, which was capable of providing the required pressure data.

For this simulation, a single rigid cylinder, 0.2 m in diameter was placed within a cuboidal domain, 1 m in length, 0.8 m wide and 0.3 m high. The cylinder height was set equal to the domain height, representing emergent flow conditions. The cylinder was represented using an immersed boundary method, with a no slip condition and a logarithmic law of the wall approximation applied at the boundary. The bed was modelled using a similar no-slip boundary condition with a logarithmic law of the wall approximation in the near-bed region. The side walls were both treated as frictionless boundaries and the free surface was modelled using a rigid-lid approach.

The grid resolution was 0.005 m in each direction (*nx*=200, *ny*=160, *nz*=60) and was chosen to ensure adequate resolution around the stem, without unnecessary CPU time restrictions. The inlet velocity was set to 0.3 ms^{-1} to ensure that the cylinder Reynolds number (Re_c=60 000) was well within the range at which the drag coefficient can be estimated as 1 (Figure 1). The flow was subcritical, with a Froude number of 0.18.

The flow was simulated using Large Eddy Simulation (LES) with a standard Smagorinsky (1963) sub-grid model. However, in order to aid convergence, the simulation was started from a converged Reynolds-Averaged Navier-Stokes (RANS) solution calculated using an RNG κ-ε turbulence model. The Navier-Stokes Equations were coupled and solved using the SIMPLEST algorithm (Patankar and Spalding, 1972). At each time-step, the flow was solved iteratively until convergence was obtained. The convergence criterion was set such that mass and momentum residuals were reduced to 0.1% of the inlet flux.

The use of LES allows time-dependent solutions to be achieved and therefore the process of turbulent energy extraction via wake-shedding to be simulated, thus providing an accurate calculation of the form drag. Furthermore, the time-dependent solution permits analysis of variation from the mean value through time.

5 BENCHMARK DRAG CALCULATION RESULTS

Here, the temporally and spatially averaged results are considered in order to assess agreement between the calculated and predicted bulk drag coefficients. The average distribution of the pressure coefficient around the cylinder (Figure 4) is consistent in shape with the idealized profiles. As expected, the pressure coefficient maximum occurs at the front of the stem, where flow deflection is greatest. A smaller peak in pressure occurs at the back of the stem, within the wake, due to the presence of recirculation cells. Pressure minima occur at the sides of the stem where velocity is greatest and flow deflection is minimal.

The values of pressure coefficient at the front of the stem agree well with the expected value of 1 within the characteristic profiles. At the sides of the cylinder, there is more discrepancy, particularly on one side, where the pressure coefficient is significantly lower than expected. Overall, the pressure value is more similar to that expected for the supercritical case. There is also noticeable variation in values within the side regions, with a significant difference in pressure between neighboring points. This may be due to the discretization process at the cylinder edge. Pressure was calculated in the boundary cells, however no allowance was made for the difference in distance between the boundary and the cell centre, at which point the pressure is evaluated, between different discrete points.

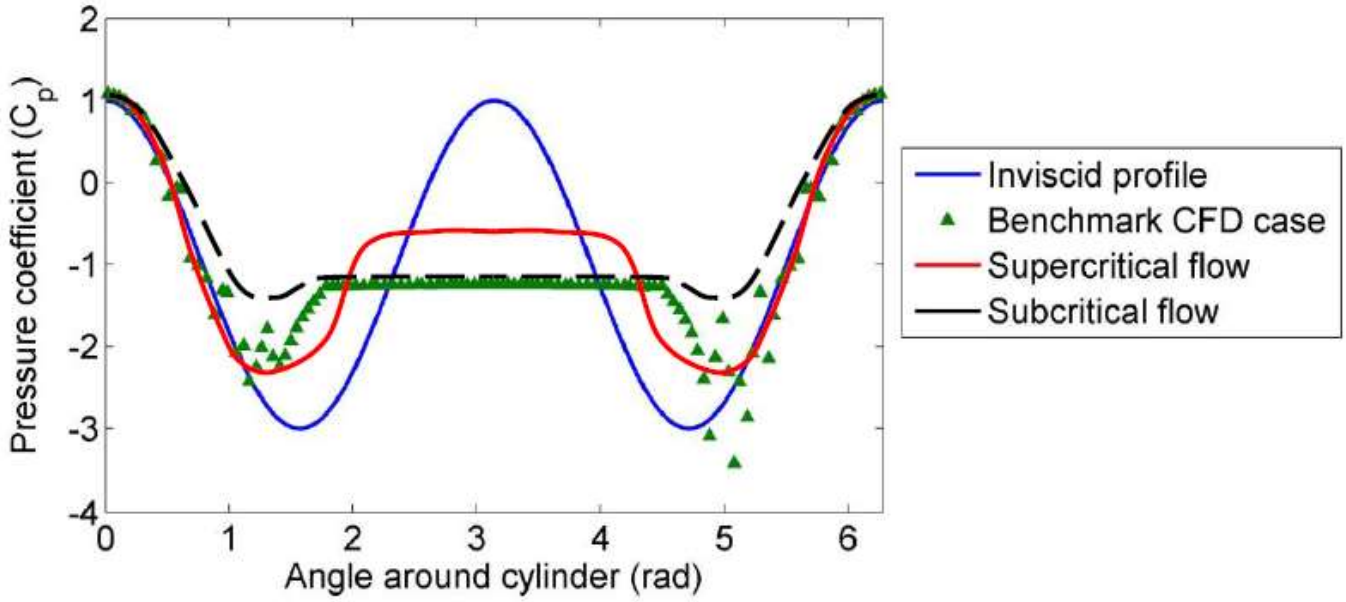

Figure 4: Pressure coefficient distribution around a cylinder for different flow conditions. Characteristic profiles taken from Anderson (1984)

However, errors at the sides of cylinder do not contribute significantly to the downstream drag due to their angle to the flow and therefore it is not anticipated that these errors will seriously affect the drag coefficient value.

In the wake, behind the stem, observed pressure values are slightly lower than expected, suggesting weaker flow recirculation than expected. This is most likely due to the limitations of the turbulence model in reproducing the full wake turbulence structure, but may also be related to the shallowness of the domain.

Using the drag calculation method described above, the spatially and temporally averaged drag coefficient for the cylinder is 0.9614, with a standard deviation, accounting for both temporal and spatial variation, of 0.0113. Assuming that the form drag accounts for 90-95% of the total drag, this mean value is in good agreement with previous experimental values, and indicates that, for this simple flow case, there is little variation in drag coefficient up the stem or through time. This is expected given the uniform inlet condition used within the simulation.

6 APPLICATION TO A FLEXIBLE STEM

Having demonstrated the accuracy of the drag back-calculation method for a simple, rigid benchmark case, the scheme was then used to simulate a flexible stem. Only a single stem was used in order to isolate the effect of the flow on vegetative drag and remove the complex feedbacks associated with flow through canopies.

In order to investigate the effect of the variable drag calculation, two similar numerical simulations were performed. Both used a biomechanical vegetation model to simulate plant motion within a CFD framework. One used a constant drag coefficient of 1, whereas the other used the dynamic drag treatment described above, calculated at each timestep.

6.1 *Simulation Setup*

For these simulations, a single stalk of vegetation was incorporated using the model of Marjoribanks *et al*. (in review), whereby the vegetation is represented using a dynamic mass flux scaling approach and plant motion is calculated using an Euler-Bernoulli beam model. With the exception of the different drag treatments, the parameters for the two simulations were identical.

The numerical domain was 0.768 m long, 0.068 m wide and 0.64 m high, with a grid resolution of 0.002 m. The stem was 0.4 m long, with a radius of 0.005 m and was placed in the centre of a domain. The rigidity of the stem was set at 0.02 Nm^2. The bed was modelled using a no-slip boundary condition with a logarithmic law of the wall approximation in the near-bed region. The side walls were both treated as frictionless boundaries and the free surface was modelled using a rigid-lid approach.

The initial inlet velocity was set at 0.7 ms^{-1} to ensure significant plant motion, with a flow Reynolds number of 23 000 and Froude number of 0.28. The cylinder Reynolds number was 7 000. Recirculating boundaries were applied in the downstream direction in order to provide a turbulent boundary condition. The simulation methods were identical to those used for the benchmark model.

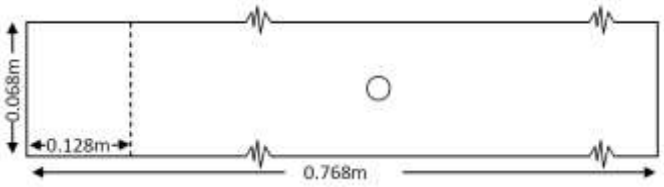

Figure 5. Numerical domain for the single stem experiments with flow from left to right. The dotted line indicates the extent of the flow recirculation region.

6.2 *Results*

As with the benchmark case, the focus here is predominantly on the time-averaged results. The mean deflected plant height for the static drag simulation was 0.3 m (75% of the original plant height). In contrast, the mean deflected plant height for the dynamic drag simulation was 0.33 m (83% of the original plant height). This demonstrates a significant difference in prediction between the two different models.

The reason for this difference becomes clear when analyzing the difference in drag coefficient between the two simulations. For the dynamic drag treatment, the spatially and temporally averaged drag coefficient was 0.91 (90% of the value used within the constant drag coefficient case). This lower drag coefficient allows the vegetation to occupy a greater height within the flow.

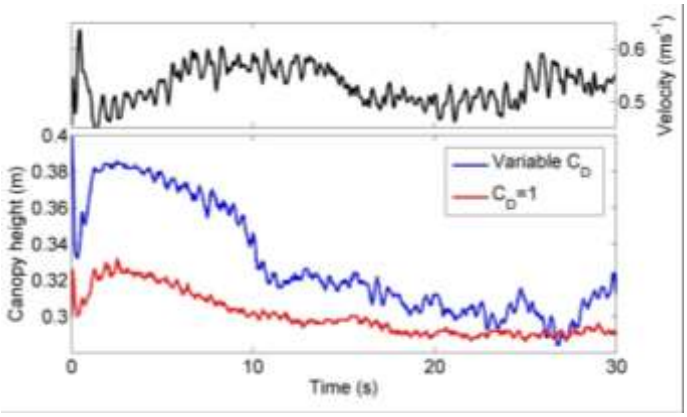

Figure 7. Canopy height time series for the constant (red) and variable (blue) drag coefficient simulations. The velocity time series for the dynamic drag coefficient simulation is shown in black.

Figure 7 shows the change in stem height during the two simulations. Two clear patterns emerge from these data. First, as shown by the mean canopy height discussed above, the constant drag coefficient leads to a lower canopy height throughout the simulation. Only at one instance (~27 s) does the constant drag coefficient correctly predict the plant height.

Second, it is clear in Figure 7 that there is far more flow-vegetation interaction within the dynamic drag case. This is shown by greater variation in height throughout the simulation, in comparison with the constant drag coefficient case which appears to reach almost equilibrium status with the flow. This difference is to be expected as the dynamic drag coefficient responds to changes in the flow and plant position, enabling feedbacks between the flow and vegetation whereas the constant drag model is much more loosely coupled to the flow conditions.

The velocity time series illustrates that the plant-flow interaction is complex. There is some evidence of velocity maxima coinciding with canopy height minima, particularly at the beginning and end of the time series. However, there are clearly a number of other factors, including plant biomechanics and initial reconfiguration which affect plant motion in addition to velocity. Nevertheless, it is clear that the dynamic drag treatment is more able to represent plant motion throughout time.

7 CONCLUSIONS

This paper has demonstrated the capabilities of a drag back-calculation method to predict, with accuracy, the drag coefficient for flow around a cylinder. The method uses the pressure data, available within high-resolution CFD modelling, in order to resolve the net force on the object. The results show the method to be highly accurate for rigid cylinders.

Application of the model to a single, flexible vegetation stem has demonstrated the inaccuracy of using a constant drag coefficient of 1 for modelling flexible vegetation. Notably, the results indicate that the mean drag coefficient is significantly lower than 1, and as a result the plant displays a more upright position within the flow, than the constant drag coefficient predicts.

Furthermore, analysis of the variation in canopy height through time reveals that in addition to predicting a lower canopy height, the constant drag coefficient also dampens the interaction between the flow and vegetation.

While the method is only used here to calculate the drag around a single stem, we argue that this methodology represents a potential step-change in our ability to model drag within vegetation canopies and inclusion of the dynamic drag calculation method within a full canopy biomechanical vegetation model is noted as an area for further development.

REFERENCES

Abdelrhman, M. A. (2007) Modeling coupling between eelgrass Zostera marina and water flow. Marine Ecology Progress Series, 338, 81-96.

Albayrak, I., Nikora, V., Miler, O. & O'hare, M. (2011) Flow-plant interactions at a leaf scale: effects of leaf shape, serration, roughness and flexural rigidity. Aquatic Sciences - Research Across Boundaries, 1-20.

Anderson, J. D. (1984) Fundamentals of Aerodynamics, New York, McGraw-Hill.

Cheng, N. (2013) Calculation of Drag Coefficient for Arrays of Emergent Circular Cylinders with Pseudofluid Model. Journal of Hydraulic Engineering, 139, 602-611.

Defina, A. & Bixio, A. C. (2005) Mean flow and turbulence in vegetated open channel flow. Water Resources Research, 41, 12.

Dijkstra, J. T. & Uittenbogaard, R. E. (2010) Modeling the interaction between flow and highly flexible aquatic vegetation. Water Resour. Res., 46, W12547.

Finnigan, J. (1979) Turbulence in waving wheat I. Mean statistics ans Honami. Boundary-Layer Meteorology, 16, 181-211.

Finnigan, J. (2000) Turbulence in Plant Canopies. Annual Review of Fluid Mechanics, 32, 519-571.

Fischer-Antze, T., Stoesser, T., Bates, P. & Olsen, N. R. B. (2001) 3D numerical modelling of open-channel flow with submerged vegetation. Journal of Hydraulic Research, 39, 303-310.

Ghisalberti, M. & Nepf, H. M. (2002) Mixing layers and coherent structures in vegetated aquatic flows. Journal of Geophysical Research-Oceans, 107, 11.

Gurnell, A. (2013) Plants as river system engineers. Earth Surface Processes and Landforms, n/a-n/a.

Ho, C. M. & Huerre, P. (1984) Perturbed Free Shear Layers. Annual Review of Fluid Mechanics, 16, 365-424.

Ikeda, S. & Kanazawa, M. (1996) Three-dimensional organized vortices above flexible water plants. Journal of Hydraulic Engineering-Asce, 122, 634-640.

Jarvela, J. (2002) Flow resistance of flexible and stiff vegetation: a flume study with natural plants. Journal of Hydrology, 269, 44-54.

Lilly, D. K. (1967) The representation of small-scale turbulence in numerical simulation experiments. IN GOLDSTINE, H. H. (Ed. IBM Scientific Computing Symp. on Environmental Sciences.

Liu, C. & Shen, Y.-M. (2008) Flow structure and sediment transport with impacts of aquatic vegetation. Journal of Hydrodynamics, Ser. B, 20, 461-468.

López, F. & García, M. (1998) open-channel flow through simulated vegetation: Suspended sediment transport modeling. Water Resources Research, 34, 2341-2352.

Lopez, F. & Garcia, M. H. (2001) Mean flow and turbulence structure of open-channel flow through non-emergent vegetation. Journal of Hydraulic Engineering-Asce, 127, 392-402.

Marjoribanks, T., Hardy, R. J., Lane, S. N. & Parsons, D. R. (in review) High resolution modelling of flow-vegetation interactions. Journal of Hydraulic Research.

Nepf, H. & Ghisalberti, M. (2008) Flow and transport in channels with submerged vegetation. Acta Geophysica, 56, 753-777.

Nepf, H., Ghisalberti, M., White, B. & Murphy, E. (2007) Retention time and dispersion associated with submerged aquatic canopies. Water Resources Research, 43, 10.

Nepf, H. M. (1999) Drag, turbulence, and diffusion in flow through emergent vegetation. Water Resources Research, 35, 479-489.

Nezu, I. & Onitsuka, K. (2001) Turbulent structures in partly vegetated open-channel flows with LDA and PIV measurements. Journal of Hydraulic Research, 39, 629-642.

Nikora, N. & Nikora, V. (2007) A viscous drag concept for flow resistance in vegetated channels. Proceedings of the 32nd Congress of IAHR. Venice.

Okamoto, T.-A. & Nezu, I. (2009) Turbulence structure and "Monami" phenomena in flexible vegetated open-channel flows. Journal of Hydraulic Research, 47, 13.

Patankar, S. V. & Spalding, D. B. (1972) A calculation procedure for heat, mass and momentum transfer in three-dimensional parabolic flows. International Journal of Heat and Mass Transfer, 15, 1787-1806.

Raupach, M. R., Finnigan, J. J. & Brunet, Y. (1996) Coherent eddies and turbulence in vegetation canopies: The mixing-layer analogy. Boundary-Layer Meteorology, 78, 351-382.

Raupach, M. R. & Thom, A. S. (1981) Turbulence in and above plant canopies. Annual Review of Fluid Mechanics, 13, 97-129.

Roshko, A. (1961) Experiments on the flow past a circular cylinder at very high Reynolds number. Journal of Fluid Mechanics, 10, 345-356.

Sand-Jensen, K. (2003) Drag and reconfiguration of freshwater macrophytes. Freshwater Biology, 48, 271-283.

Sand-Jensen, K. a. J., Jeppesen, E., Nielsen, K., Van Der Bijl, L., Hjermind, L., Nielsen, L. W. & Ivlrsln, T. M. (1989) Growth of macrophytes and ecosystem consequences in a lowland Danish stream. Freshwater Biology, 22, 15-32.

Seginer, I., Mulhearn, P. J., Bradley, E. F. & Finnigan, J. J. (1976) Turbulent flow in a model plant canopy. Boundary-Layer Meteorology, 10, 423-453.

Smagorinsky, J. (1963) GENERAL CIRCULATION EXPERIMENTS WITH THE PRIMITIVE EQUATIONS. Monthly Weather Review, 91, 99-164.

Stoesser, T., Liang, C., Rodi, W. & Jirka, G. (2006) Large eddy simulation of fully-developed turbulent flow through submerged vegetation. River Flow 2006, Two Volume Set. Taylor & Francis.

Stoesser, T., Salvador, G. P., Rodi, W. & Diplas, P. (2009) Large Eddy Simulation of Turbulent Flow Through Submerged Vegetation. Transport in Porous Media, 78, 347-365.

Sukhodolov, A. N. & Sukhodolova, T. A. (2010) Case Study: Effect of Submerged Aquatic Plants on Turbulence Structure in a Lowland River. Journal of Hydraulic Engineering, 136, 434-446.

Tritton, D. J. (1959) Experiments on the flow past a circular cylinder at low Reynolds numbers. Journal of Fluid Mechanics, 6, 547-567.

Tritton, D. J. (1988) Physical Fluid Dynamics, Oxford, Oxford University Press.

Wilson, C., Stoesser, T., Bates, P. D. & Pinzen, A. B. (2003) Open channel flow through different forms of submerged flexible vegetation. Journal of Hydraulic Engineering-Asce, 129, 847-853.

Yagci, O. & Kabdasli, M. S. (2008) The impact of single natural vegetation elements on flow characteristics. Hydrological Processes, 22, 4310-4321.

Zong, L. & Nepf, H. (2010) Flow and deposition in and around a finite patch of vegetation. Geomorphology, 116, 363-372.